

## THE CIRCUMSTELLAR H<sub>2</sub>O MASER EMISSION ASSOCIATED WITH FOUR LATE-TYPE STARS

K. J. JOHNSTON, J. H. SPENCER, AND P. F. BOWERS<sup>1</sup>

E. O. Hulburt Center for Space Research, Naval Research Laboratory, Washington, DC

Received 1984 April 5; accepted 1984 September 20

### ABSTRACT

The positions and structure of H<sub>2</sub>O masers associated with four long-period variable stars (RX Boo, R Aql, RR Aql, and NML Cyg) have been measured, using the VLA with a spatial resolution of 0".07. The H<sub>2</sub>O features appear to be unresolved knots (<0".07) distributed over not more than ~0".4. There are sometimes more than one maser condensation per synthesized beam. For the Mira variables R Aql and RR Aql the velocity and spatial structure change considerably with time, based on measurements at two epochs separated by 15 months. The estimated sizes of the H<sub>2</sub>O maser regions are ~8 × 10<sup>14</sup> for RX Boo, R Aql, and RR Aql, exceeding previous estimates for Mira variables by nearly a factor of 10. The supergiant star NML Cyg has the largest maser region (10<sup>16</sup> cm) which is comparable to that of VY CMa.

The positional accuracy for individual maser features ranges between 0".03 and 0".09 and is referenced to the position of extragalactic radio sources. However, the precise location of the maser emission relative to the stellar photocenter can be determined only at the 0".1 level because simple geometrical models for expansion do not fit the velocity and spatial distributions of the emission. Therefore, there may be difficulties when using the H<sub>2</sub>O maser emission to compare the relationship of stellar reference frames such as the FK4 to the radio reference frame defined by extragalactic radio sources at levels less than 0".1.

*Subject headings:* interferometry — masers — stars: circumstellar shells — stars: late-type — stars: long-period variables — stars: radio radiation

### I. INTRODUCTION

Studies of the maser emission associated with late-type stars are useful for examining the mass outflow in circumstellar regions. The structure and kinematics of the outer envelopes (≥100 AU) of late-type stars can be studied with the 18 cm ground-state rotational transitions of OH (Bowers, Johnston, and Spencer 1983). Because of its higher excitation requirement, the 22 GHz H<sub>2</sub>O maser probes regions of higher temperature closer to the star.

Very long baseline interferometer (VLBI) observations by Spencer *et al.* (1979) of the late-type stars RT Vir, W Hya, RX Boo, and RR Aql showed that the water vapor masers were confined to a small region near the stars (<10<sup>14</sup> cm) and had apparent core sizes of 0.5–2 × 10<sup>13</sup> cm. In contrast, the diameter of the water vapor masering region associated with the supergiant star VY CMa is ~5 × 10<sup>15</sup> cm (Rosen *et al.* 1978).

To extend the VLBI results, we have observed four late-type stars with strong H<sub>2</sub>O masers in order to map the distribution of the emission with a lower spatial resolution (~0".07) and to obtain precise positions of the masers which we subsequently compare to other high-quality positions. The stars observed include the Mira variables R Aql and RR Aql, which are conveniently close to each other in the sky, the SRb semiregular variable RX Boo, and the supergiant star NML Cygnus.

### II. THE OBSERVATIONS

The stars were observed using the Very Large Array of the National Radio Astronomy Observatory<sup>2</sup> in the standard A configuration. On 1981 January 9 R Aql, RR Aql, and NML

Cyg were observed for five scans of 20 minutes each. On 1982 March 22, RX Boo, R Aql, and RR Aql were observed for seven to eighteen scans of 12 minutes each along with observations of nearby calibrators. The 1981 data were taken in left circular polarization, while in 1982 right circular polarization was used. All the observations used a total bandwidth of 3.125 MHz (42.2 km s<sup>-1</sup>). In 1982, 64 spectral channels with a resolution of 1.3 km s<sup>-1</sup> were used; in 1981 128 spectral channels doubled the resolution to 0.66 km s<sup>-1</sup> after Hanning weighting. In 1982 March, 12 antennas were used with spacings ranging from 47 to 2.5 × 10<sup>3</sup> kλ. In 1981 January, nine antennas were used with spacings ranging from 41 to 1.8 × 10<sup>3</sup> kλ. The lower spectral resolution and greater number of antennas resulted in an improved dynamic range for the 1982 data. The flux density scale was established by assuming the flux density of 3C 286 to be 2.55 Jy at 22.2 GHz (Baars *et al.* 1977). The data were reduced in the standard manner using nearby calibrators to establish the system phase and amplitude. The positions of Witzel and Johnston (1982) were assumed for the calibrators. The data were then self-calibrated using the AIPS (Astronomical Image Processing System) as it existed in 1982 March.

### III. RESULTS

#### a) Presentation of the Maps

In this section profiles and maps of the H<sub>2</sub>O emission from each star are presented. All spectral profiles were obtained by scalar averaging only the short baseline data. Maps are presented for velocities where the emission was resolved into more than one spatial component. The velocity with respect to the local standard of rest and the peak map flux density (janskys per beam) are given in the upper left corner of each map.

<sup>1</sup> Also at Sachs/Freeman Associates, Bowie, MD 20715.

<sup>2</sup> The National Radio Astronomy Observatory is operated by Associated Universities, Inc., under contract with the National Science Foundation.

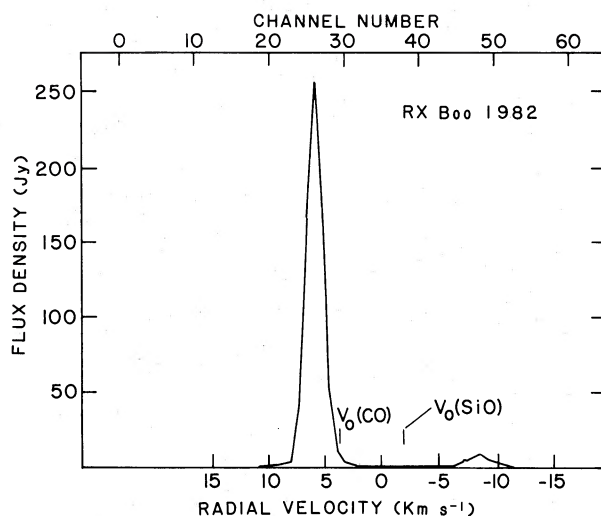


FIG. 1a.— $\text{H}_2\text{O}$  spectrum of RX Boo at epoch 1982.2. The LSR velocities are based on a rest frequency of 22235.080 for the  $5_{16} \rightarrow 6_{16}$  transition of  $\text{H}_2\text{O}$ . The velocity resolution is  $1.3 \text{ km s}^{-1}$ . Every other channel is independent, since Hanning weighting was used.

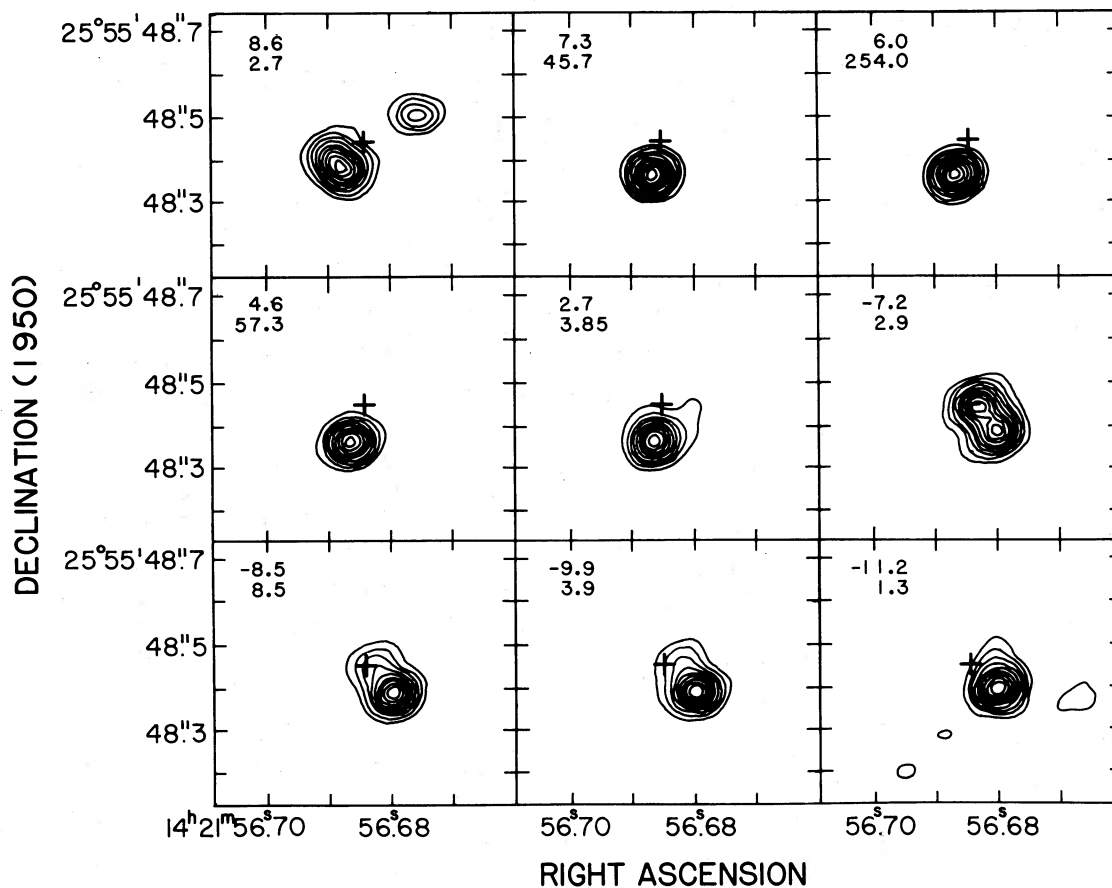


FIG. 1b.—Maps of individual channels of the spectrum displayed in Fig. 1. The center velocity and peak flux density per beam are presented in the right-hand corner of the individual maps. The contour levels are  $-1\%$ ,  $1\%$ ,  $2\%$ ,  $3\%$ ,  $4\%$ ,  $5\%$ ,  $6\%$ ,  $7\%$ ,  $8\%$ ,  $9\%$ , and  $100\%$  of the peak flux density per beam. The feature at  $7.3 \text{ km s}^{-1}$  is unresolved and is typical of the synthesized beam. The coordinates of right ascension and declination are not current in an absolute sense since the data were self calibrated, but the relative positions from map to map are correct. The cross represents a fiducial for comparison of the maps.

i) *RX Boo*

During 1982 March, RX Boo's  $\text{H}_2\text{O}$  emission ranged from  $-10$  to  $+9 \text{ km s}^{-1}$  with strong peak emission at  $6 \text{ km s}^{-1}$ . Figure 1a shows the average emission observed over the short spacings less than  $5 \text{ k}\lambda$ . Maps at individual velocities are displayed in Figure 1b and indicate that the  $\text{H}_2\text{O}$  emission is spread over  $\sim 0''.2$  among three principal condensations. The features at  $7.3$  through  $4.6 \text{ km s}^{-1}$  are single unresolved features and represent the response of the VLA to a single point source. At other radial velocities, the maps may be represented by two to three components. The map at  $8.6 \text{ km s}^{-1}$  may be modeled as three components. Two of these three components make up the strong  $2.7 \text{ Jy}$  source at  $8.6 \text{ km s}^{-1}$ . There may be other spatial features. The dynamic range of the maps is of order 100:1. There may be weak features present in the emission that are below the level of the dynamic range of the maps.

ii) *R Aql*

This source was observed in 1981 and 1982. The spectra for 1981 January and 1982 March are displayed in Figure 2. Peak emission occurs at  $50.4$ ,  $48.0$ ,  $45.8$ , and  $40.8 \text{ km s}^{-1}$ . The maps of this emission are shown in Figures 3a and 3b for 1981 and 1982, respectively. There is emission distributed over  $0''.3$ . In 1981, the emission was dominated by two centers of activity separated by  $0''.11$  along p.a.  $\approx 140^\circ$ , as is evident from the  $49.0 \text{ km s}^{-1}$  map. The southern component appears to be present at all velocities, but the northern component is present only at  $v \geq 47 \text{ km s}^{-1}$ . The emission in 1982 also appears to consist of

two dominant components. Inspection of the  $48.0 \text{ km s}^{-1}$  map shows the component separation to be  $0''.12$  at p.a.  $= -73^\circ$ . The absolute position of the 1981 map is not well determined, but the change in component separation and position angle suggest that the emission structure at a given velocity may have varied slightly between the two epochs.

iii) *RR Aql*

Figure 4 displays the  $\text{H}_2\text{O}$  spectra for 1981 and 1982. The structure and velocity range of the emission has changed quite noticeably between the two epochs. The dominant spectral features in the 1981 spectrum are at  $27.3$  and  $25.3 \text{ km s}^{-1}$ , but in the 1982 spectrum there are features at  $34.8$ ,  $29.4$ , and  $26.5 \text{ km s}^{-1}$ . Maps are shown in Figure 5 only for epoch 1981. The maps for epoch 1982 are not shown because little or no extended emission is seen at any velocity. Some of the maps in Figure 5, especially at  $27.3 \text{ km s}^{-1}$ , appear to be resolved but may be modeled as spatial blends of two components separated by less than a beamwidth.

iv) *NML Cyg*

The spectrum of the  $\text{H}_2\text{O}$  emission associated with the supergiant NML Cygnus is displayed in Figure 6, together with maps of the relevant channels. This emission is distributed over an angular scale of  $0''.4$  with the low-velocity ( $-20$  to  $-15 \text{ km s}^{-1}$ ) emission extended over an area of  $\sim 0''.2$  and separated from the weak, unresolved high-velocity ( $5 \text{ km s}^{-1}$ ) emission by  $0''.35$  along a position angle of  $-50^\circ$ . The emission appears to be two-sided, since the  $-15.5$  and  $5.9 \text{ km s}^{-1}$  maps display emission of almost equal flux density. The features at  $-16.8$  and  $-15.5 \text{ km s}^{-1}$  appear to be quite complex, but may be represented by a maximum of three components.

Inspection of light curves (Mattei 1984) for RX Boo, R Aql, and RR Aql, and using the periods and epochs reported for R Aql, RR Aql, and NML Cyg by Herman (1983), indicates that for the 1981 January 9 observations the light curve of R Aql was at phase 0.99 and magnitude  $6.2V$ , RR Aql was at phase 0.08, while NML Cyg was at phase 0.74. On 1982 March 22 R Aql was at phase 0.55 and magnitude  $10.6V$ , RR Aql was at phase 0.16, and RX Boo was at magnitude  $7.7V$ . The maser flux density for R Aql is 4 times as intense at phase 0.99 than at phase 0.55. The maser emission appears to be spread out over a larger area at phase 0.55. This may be due to real motion or may simply be due to the dynamic range of the maps.

b) *Source Positions*

The position of a bright compact maser feature for each star is given in Table 1. In the case of RX Boo, RR Aql, and NML Cyg the spectral feature whose position was measured appears to be a single maser feature at a dynamic range of 20:1. The feature used in RR Aql had a flux density of  $2.5 \text{ Jy}$ . In the case of R Aql, the  $40.1 \text{ km s}^{-1}$  feature was chosen which may be represented as a double with a 20:1 flux density ratio, as seen by inspection of Figure 3b. The second column is the radial velocity of the maser feature. The third column is the flux density of the feature. The fourth column is the right ascension and declination of the maser feature. Columns (6), (7), and (8) list the calibrator, its right ascension, and its declination, respectively. These positions are the sum of the measured arc between the calibrator and the maser emission, where the adopted position of the calibrator is listed in Witzel and Johnston (1982). As such, these positions are based on the extragalactic radio source reference frame defined by the catalog of Witzel and Johnston (1982). In relating these positions to the

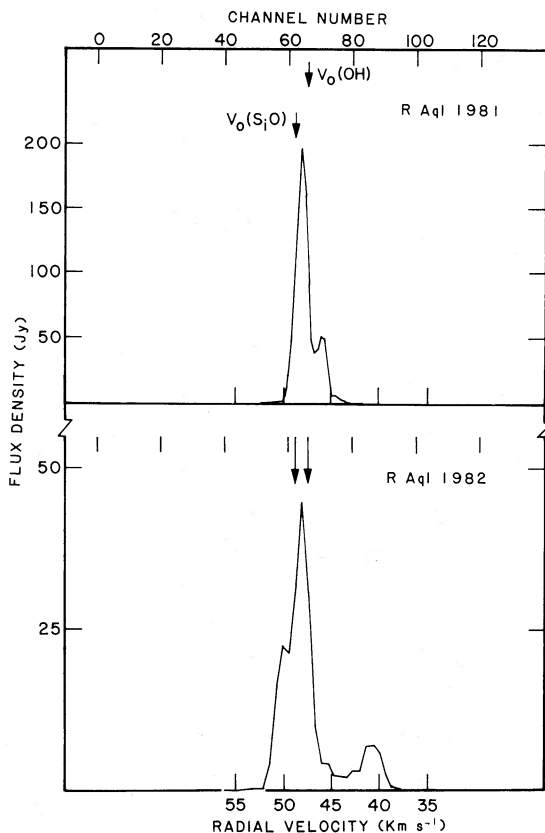


FIG. 2.— $\text{H}_2\text{O}$  spectrum of R Aql for epoch (a) 1981.0 and (b) 1982.2. The velocity resolution is  $0.66$  and  $1.3 \text{ km s}^{-1}$  for 1981 and 1982, respectively. The velocities are with respect to LSR.

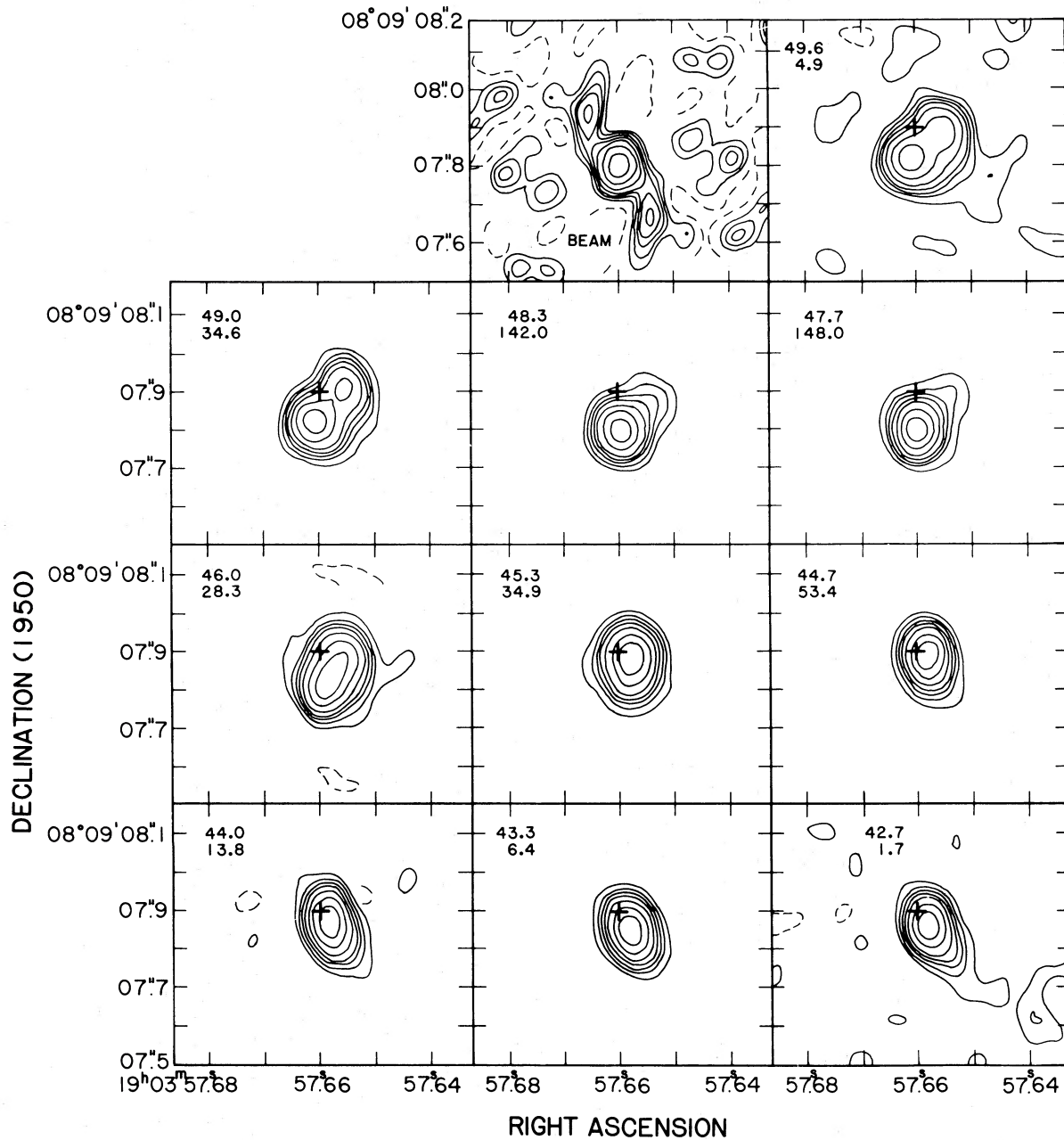


FIG. 3a.—Maps of individual channels of the spectrum of R Aql in 1981. The contour levels are  $-5\%$ ,  $5\%$ ,  $10\%$ ,  $15\%$ ,  $20\%$ ,  $30\%$ ,  $50\%$ , and  $75\%$  of the peak flux density per beam. Other comments are as in Fig. 1b.

optical stellar positions, two questions immediately arise. (1) Where is the maser feature in Table 1 located with respect to the stellar photosphere? This question is discussed in § IVc. (2) What is the relationship of the position of the calibrators used in this study to the optical FK4 system? From a comparison of the optical and radio positions of 28 extragalactic radio sources listed in Witzel and Johnston (1982), de Vegt and Gehlich (1982) find that there are discrepancies of  $0''.2$  between the optical FK4 system and the radio positions. These two error sources are not included in the positional errors listed in Table 1.

The errors listed in Table 1 are the sum of (1) errors in measuring the arc length between the maser position and calibrator and (2) the error in the calibrator position as listed in

Witzel and Johnston (1982). Only in the case of RX Boo did the position errors of its calibrator 1404+286 significantly contribute to the error listed in Table 1. The error in determining the arc length between the maser and calibrator can be expressed as an effective baseline error. The baselines are conservatively estimated to have random errors of 0.1 nanosecond which are caused mainly by tropospheric phase noise during the observations and the previous estimate of the baselines.

Although it is not possible to obtain a 1981 position for R Aql and RR Aql relative to 1741-038 because of calibration problems, we can measure their relative 1981 position and compare it to the 1982 relative position. When the apparent motion is changed to an annual rate, we obtain a proper motion measurement of R Aql relative to RR Aql of  $\Delta\alpha =$

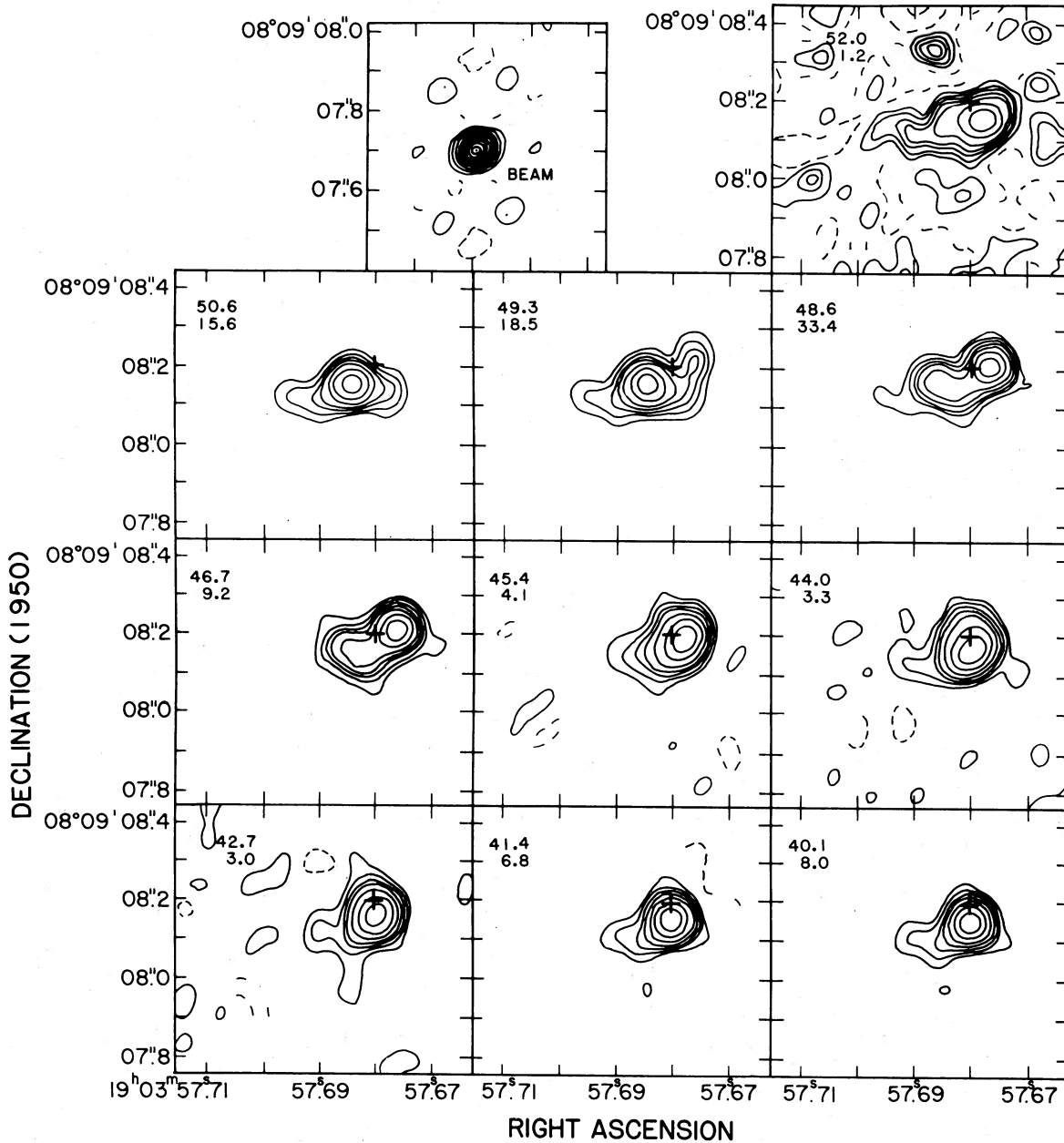


FIG. 3b.—Maps of individual channels for the spectrum of R Aql in 1982. The contour levels are the same as Fig. 3a. Other comments are as in Fig. 1b.

$0^{\circ}001 \pm 0^{\circ}002 \text{ yr}^{-1}$  and  $\Delta\delta = -0^{\circ}03 \pm 0^{\circ}05 \text{ yr}^{-1}$ . With only  $\sim 1$  yr between the observations, this is only an upper limit, but it is consistent with the cataloged values, and the method shows promise of obtaining an improved value in a few years.

#### IV. DISCUSSION

##### a) Sizes of the Emission Regions

In Table 2 we list for each star the estimated distance, characteristic angular size of the  $\text{H}_2\text{O}$  maser region, and the corresponding linear size. Distances to R Aql and RR Aql have been estimated by Bowers and Hagen (1984) from a period-luminosity-spectral class relation. RX Boo is a semiregular variable without a well-defined period; the distance is estimated by assuming a bolometric luminosity of  $10^4 L_{\odot}$  (Knapp *et al.* 1982). The distance to the supergiant NML Cyg is based

upon the distance to the Cyg OB2 association (Morris and Jura 1983; Bowers, Johnston, and Spencer 1983). Estimated errors are  $\sim 20\%$ .

Table 2 shows that the  $\text{H}_2\text{O}$  is distributed over regions ranging from  $\sim 45$  to 720 AU in size. The linear extent of the  $\text{H}_2\text{O}$  maser region is largest for the supergiant NML Cyg, and it is comparable in diameter to that of  $\sim 300$  AU found for the supergiant VY CMa (Rosen *et al.* 1978). The size of the maser region associated with the Mira variable RR Aql was previously estimated to be  $\leq 10^{14}$  cm (Spencer *et al.* 1979). This estimate is too small because only the strongest spectral feature was detected with an angular resolution of  $0^{\circ}010$ . In addition, none of the spectral features in R Aql (peak flux = 240 Jy) were detected by Spencer *et al.* (1979), indicating that the apparent sizes of some of the individual masers are larger than  $0^{\circ}010$ .

TABLE 1  
ABSOLUTE POSITIONS FOR COMPACT MASER FEATURES MEASURED AT JD EPOCH 1982.22<sup>a</sup>

Star	Velocity (km s <sup>-1</sup> )	S (Jy)	Right Ascension <sup>b</sup> (1950)	Declination <sup>b</sup> (1950)	Calibrator	$\alpha$ (1950)	$\delta$ (1950)
RX Boo .....	6.0	254	14 <sup>h</sup> 21 <sup>m</sup> 56 <sup>s</sup> .718 ± 0 <sup>o</sup> 002 56.729 ± 0.002 <sup>c</sup>	+25 55 47 <sup>o</sup> .17 ± 0 <sup>o</sup> 03 47.24 ± 0.05 <sup>c</sup>	1404 + 286	14 <sup>h</sup> 04 <sup>m</sup> 45 <sup>s</sup> .615 ± 0 <sup>o</sup> 002	+28 41 <sup>o</sup> 29 <sup>o</sup> .22 ± 0 <sup>o</sup> 02
R Aql .....	40.1	8.0	19 03 57.691 ± 0.004 57.67 ± 0.01 <sup>d</sup> 57.685 ± 0.003 <sup>e</sup>	+08 09 08.13 ± 0.08 07.7 ± 0.3 <sup>d</sup> 08.01 ± 0.07 <sup>e</sup>	1741 - 38	17 41 20.6180 ± 0.0006	-03 48 48.918 ± 0.014
RR Aql .....	23.7	2.5	19 55 00.327 ± 0.005 00.30 ± 0.01 <sup>d</sup> 00.293 <sup>f</sup>	-2 01 17.01 ± 0.09 17.1 ± 0.3 <sup>d</sup> 16.83 <sup>f</sup>	1741 - 38		
NML Cyg .....	-17.8	13.3	20 44 33.853 ± 0.005 33.84 ± 0.03 <sup>d</sup>	+39 55 57.25 ± 0.05 57.1 ± 0.3 <sup>d</sup>	2200 + 420	22 00 39.3619 ± 0.0004	+41 02 08.590 ± 0.006

<sup>a</sup> NML Cyg was measured at epoch 1981.02.

<sup>b</sup> These positions do not contain any correction for proper motion and are for the epochs given.

<sup>c</sup> Optical position epoch 1983.40 (Baudry, Mazurier, and Requeme 1983).

<sup>d</sup> Positions of star obtained from OH maser emission by Bowers, Johnston, and Spencer 1983 at epoch 1980.9.

<sup>e</sup> Position measured at epoch 1982.5 by Dick and Holdren 1984.

<sup>f</sup> Position measured at epoch 1979.75 proper motion poorly known (Soulie and Baudry 1983).

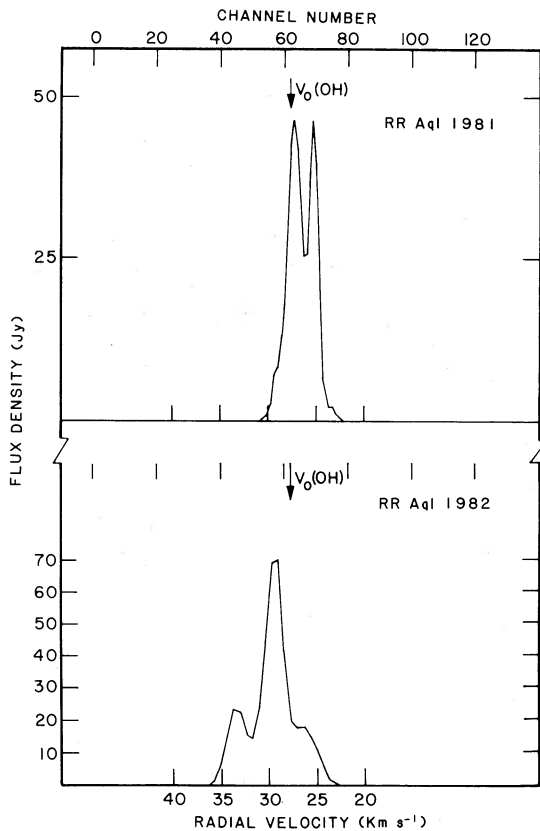


FIG. 4.— $\text{H}_2\text{O}$  spectrum for RR Aql in (a) 1981.0 and (b) 1982.2. The velocity resolution is  $0.66$  and  $1.3 \text{ km s}^{-1}$  for 1981 and 1982, respectively. The velocities are with respect to LSR.

The VLA maps show all the features to a level of  $1 \text{ Jy}$ . At this level, the diameters of the maser regions for Mira variables appear to be  $\sim 8 \times 10^{14} \text{ cm}$  if the sizes of R Aql and RR Aql measured here are representative. If the size of Mira which has been determined from speckle interferometry to have a diameter of  $3.2 \times 10^{13} \text{ cm}$  (Bonneau *et al.* 1982) is typical of Mira variables, then the maser region is 20 times the stellar diameter. Using the mass-loss rates and velocity of expansion from Bowers, Johnston, and Spencer (1983), the average  $\text{H}_2$  density of the maser regions is  $3 \times 10^7$ ,  $7 \times 10^7$ , and  $9 \times 10^6 \text{ cm}^{-3}$  for R Aql, RR Aql, and NML Cyg, respectively. The outer radius of the 1612 OH maser regions (Bowers, Johnston, and Spencer 1983) are 1200, 400, and 5400 AU for R Aql, RR Aql, and NML Cyg, respectively. Thus the OH maser region is 15–50 times larger than the  $\text{H}_2\text{O}$  maser region.

The  $\text{H}_2\text{O}$  masers are located outside the estimated conden-

TABLE 2  
CHARACTERISTICS SIZES OF  $\text{H}_2\text{O}$  MASER REGIONS

Star	Distance (pc)	Angular Diameter	Linear Diameter (A.U.)
RX Boo .....	225 <sup>a</sup>	$0''.2$	45
R Aql .....	170 <sup>b</sup>	0.3	51
RR Aql .....	560 <sup>b</sup>	$\sim 0.1$	56
NML Cyg .....	1800 <sup>c</sup>	0.4	720

<sup>a</sup> Knapp *et al.* 1982.

<sup>b</sup> Bowers and Hagen 1984.

<sup>c</sup> Bowers, Johnston, and Spencer 1983.

sation radius ( $\sim 10 \text{ AU}$ ) for silicate-type dust grains believed to be present in these oxygen-rich envelopes. The relatively large radii at which the  $\text{H}_2\text{O}$  masers are located, combined with the correlation of the microwave  $\text{H}_2\text{O}$  flux with the optical/infrared light curves (Schwartz, Harvey, and Barrett 1974), may suggest an infrared pumping mechanism. An alternative model of collisional pumping (Deguchi 1977) predicts that the  $\text{H}_2\text{O}$  masers should be located much closer ( $\lesssim 2 \text{ AU}$ ) to the star. However, the  $\text{H}_2\text{O}$  masers are located sufficiently close to the central stars that a different model of collisional pumping may be possible (see Cox and Parker 1978).

#### b) Structure of the Emission Regions

The  $\text{H}_2\text{O}$  emission probably occurs as unresolved knots ( $< 0''.1$ ) distributed over not more than a few tenths of an arc second. Each of the maps presented may be modeled by three or less components. Some of the components are spatially blended because their separation is less than a beamwidth ( $0''.07$ ). There is no clear indication for extended emission with the present spatial resolution and dynamic range.

The clumpy nature of the  $\text{H}_2\text{O}$  maps complicates the interpretation. In addition, the profiles demonstrate that the structure and velocity range of  $\text{H}_2\text{O}$  emission can vary considerably with time. Thus, data obtained at a given epoch do not necessarily reflect the entire velocity range of the  $\text{H}_2\text{O}$  region. Table 3 summarizes the velocity ranges for  $\text{H}_2\text{O}$ , as well as estimates of the systemic radial velocity  $V_0$  and the velocity ranges for transitions associated with molecules distributed in the outer envelope. For R Aql and NML Cyg, the detected velocity range for  $\text{H}_2\text{O}$  is considerably less than for SiO or OH. For R Aql and RR Aql, temporal variations of as much as a factor of 2 in the velocity ranges are evident from comparison of  $\text{H}_2\text{O}$  data at two epochs. It is clear that the profiles and maps at any given epoch must be interpreted with caution.

To determine how the data presented in the maps may be related to the underlying geometry and kinematics and to the stellar position, we summarize in Figure 7 the positions and velocities of all map features for the three stars RR Aql, R Aql, and RX Boo. Crosses in Figure 7 represent velocities  $V$  approximately equal to the stellar radial velocity  $V_0$  to within the uncertainties given in Table 2. Filled and empty circles, respectively, represent features with  $V < V_0$  or  $V > V_0$ ; filled and empty triangles represent the extreme low and high velocity features.

In a spherical outflow expanding at a constant velocity, the positions of the extreme low and high velocity features should be coincident at the position of the star; features at  $V \approx V_0$  should be distributed in ringlike structures centered at the stellar position. There is good evidence from high-resolution OH data that this model is correct, to first order, for the outer ( $> 1000 \text{ AU}$ ) envelopes of most late-type stars (Bowers, Johnston, and Spencer 1983). Evidence for this model is not as apparent for the  $\text{H}_2\text{O}$  data. Figure 7 shows that there are not significant differences between the extent over which low, middle, or high velocity ranges are distributed. The dramatic changes with time in the velocity range and map structure for R Aql and RR Aql demonstrate the difficulties of interpretation imposed by the variable emission. Good positions relating maps at different epochs are needed to obtain the complete velocity structure of the circumstellar shell. For example, the overall distribution for R Aql appears to be elongated at each epoch, but the position angle and size of the region are different.

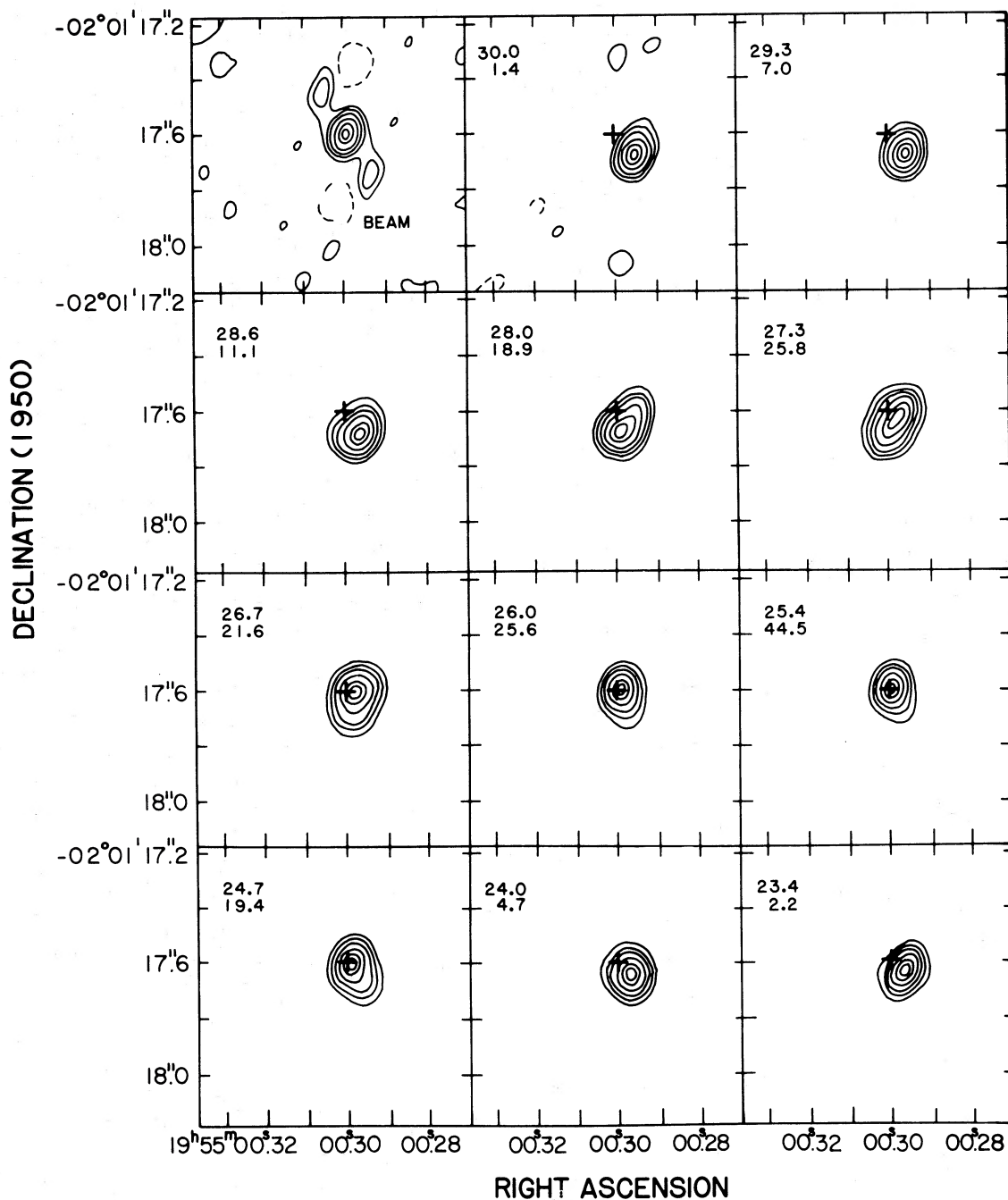


FIG. 5.—Individual channel maps for RR Aql for epoch 1982.0. The contour levels are the same as Fig. 1b. Other comments are as in Fig. 1b.

Both maps for R Aql show a tendency for the low-velocity emission to be distributed over a smaller angular extent than the high-velocity emission. We interpret this as evidence that the dominant kinematic mode is expansion. The velocity range of the H<sub>2</sub>O emission is biased toward the low-velocity end of the entire velocity range detected for thermal SiO and 1612 MHz OH (Table 3). The so-called high-velocity H<sub>2</sub>O features are actually very near the estimated stellar radial velocity, and thus should have the largest angular distribution. However,

there are probably significant transverse or radial velocity gradients (e.g., turbulence) in the region. The extreme low velocity emission for 1981 is near the center for the overall distribution, but the 1982 data show two components at an even lower velocity.

For NML Cyg there is evidence from the OH data of an underlying spherical, expanding geometry severely perturbed by the ambient interstellar UV radiation field (Bowers, Johnston, and Spencer 1983). If this is the case for the H<sub>2</sub>O region,

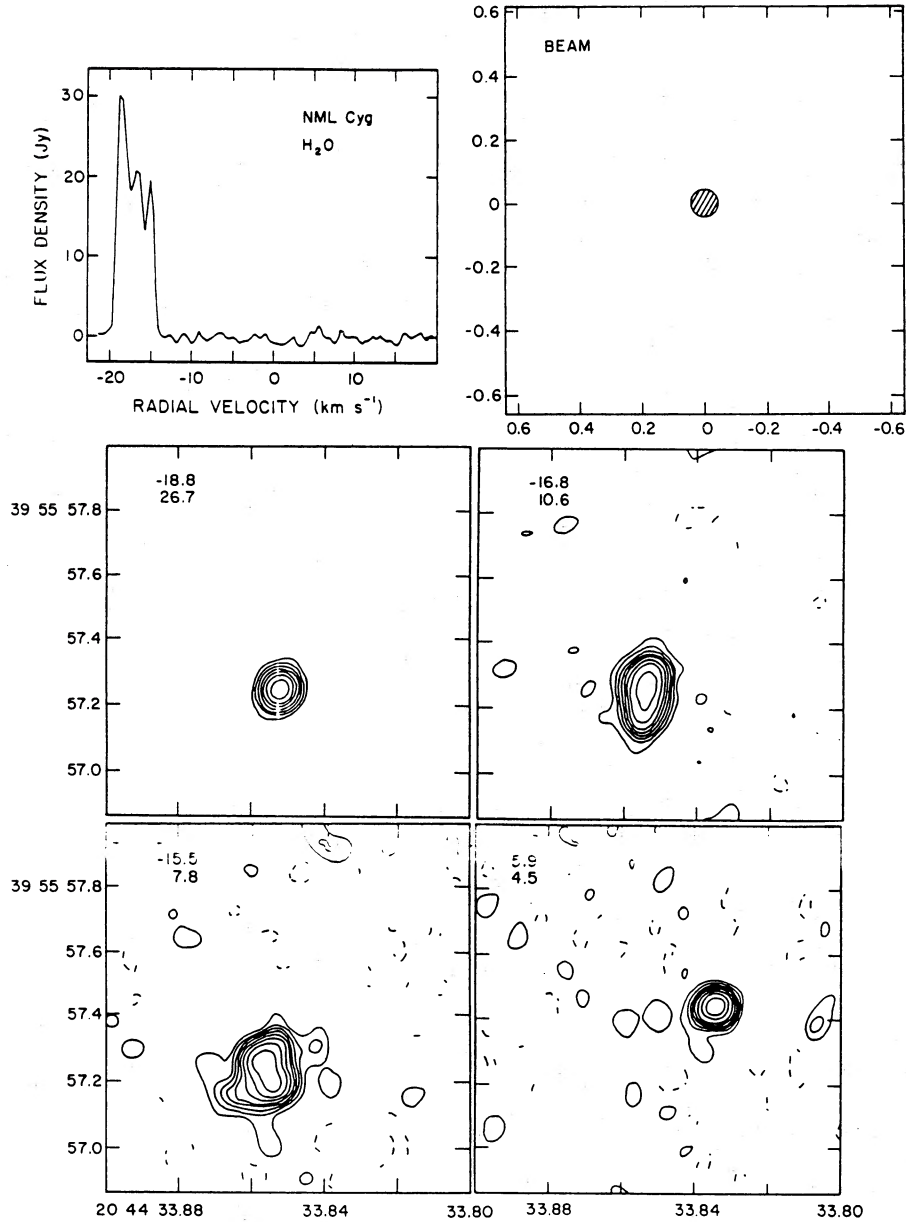


FIG. 6.— $\text{H}_2\text{O}$  emission associated with NML Cygnus (epoch 1980.0). The intensity profile as obtained using the 0.8 km baseline at 22235 MHz is displayed as a function of LSR radial velocity. The VLA maps have contour levels of  $-5\%$ ,  $5\%$ ,  $10\%$ ,  $15\%$ ,  $20\%$ ,  $25\%$ ,  $35\%$ ,  $50\%$ , and  $75\%$  of the maximum. The velocity resolution of each map is  $0.66 \text{ km s}^{-1}$ . Other comments are as in Fig. 1b.

the low-velocity components in Figure 7 are likely to be near the stellar position determined from the OH data. The velocity of the high-velocity component ( $5.9 \text{ km s}^{-1}$ ) is near the stellar velocity (Table 3), consistent with its large positional offset from the low-velocity features.

In summary, the velocity and the spatial structure of  $\text{H}_2\text{O}$  emission vary strongly as a function of time. Our data are consistent in some respects with expanding, spherical outflow but certainly do not rule out more complicated kinematic or geometric models. For example, significant velocity gradients may exist caused by turbulence or radial acceleration of the gas to its terminal velocity. In some cases (e.g., R Aql) the geometry of the region may be nonspherical; in other cases (e.g., NML Cyg) the  $\text{H}_2\text{O}$  data alone tells us very little about the underlying geometry or kinematics. It is evident that observations at

a large number of epochs will be needed to understand the nature of the  $\text{H}_2\text{O}$  regions.

#### c) Positions of the Stars

The positions of the  $\text{H}_2\text{O}$  emission features should be very close to the stellar photocenter which is presumably located somewhere within the maser region. The optical positions which are listed in Table 1 thus should lie somewhere in the maser region. However, as stated earlier, the maser positions are based upon the radio reference frame defined by the catalog in Witzel and Johnston (1982), while the optical positions are based upon the FK4 stellar reference frame. The relationship of the FK4 with the radio reference frame has not yet been established. At best the two reference frames may be coincident within  $0''.1$ – $0''.3$ . Comparison of the optical and radio positions

TABLE 3  
COMPARISON OF VELOCITY RANGES FOR VARIOUS SPECIES

Star	Species	$V_0$ (km s <sup>-1</sup> )	Velocity Range (km s <sup>-1</sup> )	Reference
RX Boo .....	H <sub>2</sub> O	...	-11.2, +8.6	1
	SiO	-2.0 ± 1.0	-13.7, +9.7	2
	CO	+3.8 ± 1.0	-4.0, +11.6	3
R Aql .....	H <sub>2</sub> O (1981)	...	+43.7, +49.6	1
	H <sub>2</sub> O (1982)	...	+40.1, +50.6	1
	SiO	+48.7 ± 0.8	+37.0, +60.4	2
	OH	+47.4 ± 1.0	+39.2, +55.6	4
RR Aql .....	H <sub>2</sub> O (1981)	...	+23.4, +29.6	1
	H <sub>2</sub> O (1982)	...	+19.7, +36.9	1
	OH	+27.8 ± 1	+21.0, +34.6	4
NML Cyg .....	H <sub>2</sub> O	...	-19, +6	1
	SiO	+4.3 ± 1.0	-25.1, +33.7	2
	SiO	-2.0 ± 1.3	-29.5, +25.5	5
	OH	-1.2 ± 1	-28.9, +26.5	4

REFERENCES.—(1) This paper; (2) Morris *et al.* 1979; (3) Knapp *et al.* 1982; (4) Bowers, Johnston, and Spencer 1983; (5) Wolff and Carlson 1982.

at this level is satisfactory but, unfortunately, does not locate the star in the maser emission region. These positions do *not* contain the effects of the proper motions of the stars. We have been very careful to present optical and radio positions measured at epochs close in time. The proper motion of R Aql is known to be 0<sup>o</sup>.002 yr<sup>-1</sup> in right ascension and -0<sup>o</sup>.069 yr<sup>-1</sup> in

declination. Since the maximum separation of the optical and radio measurements is 3 yr (RR Aql), the lack of proper motions should contribute on the 0<sup>o</sup>.1 scale when comparing positions.

Accurate positions of three of the stars have been obtained from OH maser emission by measuring the position of the extreme velocity features. Table 1 shows that the OH positions agree with the optical and the H<sub>2</sub>O maser positions at about the 0<sup>o</sup>.1 level. The OH positions also are referenced to the radio reference frame. Improved accuracy (<0<sup>o</sup>.05) in the OH stellar positions could allow us to place the position of the star within the H<sub>2</sub>O maser emission independent of optical measurements since both the OH and H<sub>2</sub>O measurements are referred to the extragalactic radio reference frame.

From the errors of the radio and optical positions presented here, measurements of a large number of stellar H<sub>2</sub>O masers at several epochs together with their optical positions could eventually define the relationship of the FK4 with the radio reference frame at the ~0<sup>o</sup>.1 level over the entire sky. From this study we see no reason to place the star at any particular position in the maser region, which for these stars is a few tenths of an arc second in extent (see Fig. 7). Detailed models of the geometry and velocity fields of H<sub>2</sub>O masers will be needed to determine the position of the star in the maser region in order to relate the optical and radio reference frames at levels ≤0<sup>o</sup>.1.

## V. CONCLUSIONS

High-resolution (0<sup>o</sup>.07) observations of H<sub>2</sub>O maser emission associated with four stars have revealed that (a) the maser features generally are unresolved and are distributed over linear diameters ranging from 45 to 720 AU; (b) a simple model of constant expansion does not fit the velocity/spatial distribution of the emission; (c) the location of the maser emission relative to the optical photocenter is difficult to determine at levels of 0<sup>o</sup>.1.

We acknowledge the AAVSO observational data sent to us by the director, Janet A. Mattei.

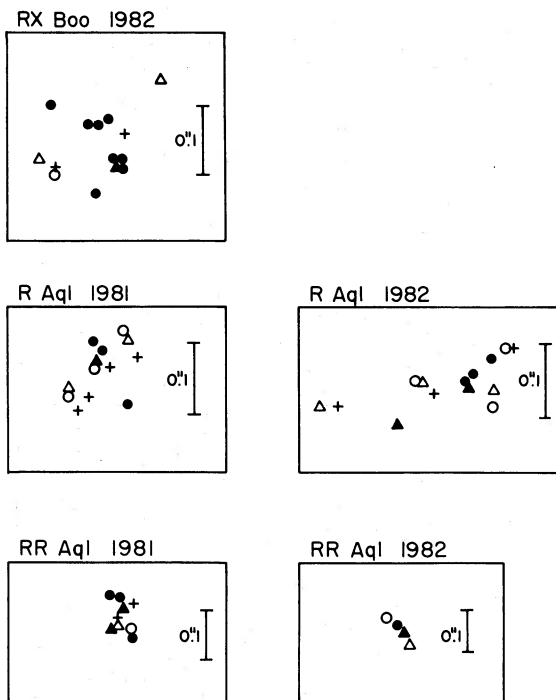


FIG. 7.—Summary of the positions and velocities of the H<sub>2</sub>O features for the stars RX Boo, R Aql, and RR Aql. Crosses indicate velocities approximating the stellar radial velocity  $V_0$ . Filled or empty circles represent features with velocities  $V < V_0$  and  $V > V_0$ , respectively. Filled and empty triangles represent the extreme low and high velocity features.

## REFERENCES

- Baars, J. W. M., *et al.* 1977, *Astr. Ap.*, **61**, 99.  
 Baudry, A., Mazurier, J. M., and Requieme, Y. 1983, in *IAU Symposium 110, VLBI and Compact Radio Sources*, ed. R. Fanti, K. I. Kellermann, and G. Setti (Dordrecht: Reidel), p. 355.  
 Bonneau, D., Foy, K., Blazit, A., and Labeyrie, A. 1982, *Astr. Ap.*, **106**, 235.  
 Bowers, P. F., and Hagen, W. 1984, *Ap. J.*, **285**, 637.  
 Bowers, P. F., Johnston, K. J., and Spencer, J. H. 1983, *Ap. J.*, **274**, 733.  
 Cox, G. G., and Parker, E. A. 1978, *M.N.R.A.S.*, **183**, 111.  
 Deguchi, S. 1977, *Publ. Astr. Soc. Japan*, **29**, 669.  
 de Vegt, Ch., and Gehlick, U. K. 1982, *Astr. Ap.*, **113**, 213.  
 Dick, S. J., and Holdenreid, E. R. 1984, private communication.  
 Herman, J. 1983, Ph.D. thesis, Sterrewacht Leiden.  
 Knapp, G. R., Phillips, T. G., Leighton, R. B., Lo, K. Y., Wannier, P. G., and Wootten, H. A. 1982, *Ap. J.*, **252**, 616.  
 Mattei, J. A. 1984, private communication.  
 Morris, M., and Jura, M. 1983, *Ap. J.*, **267**, 179.  
 Morris, M., Redman, R., Reid, M. J., and Dickinson, D. F. 1979, *Ap. J.*, **229**, 257.  
 Rosen, B. R., *et al.* 1978, *Ap. J.*, **222**, 132.  
 Schwartz, P. R., Harvey, P. M., and Barrett, A. H. 1974, *Ap. J.*, **187**, 491.  
 Soule, G., and Baudry, A. 1983, *Astr. Ap. Suppl.*, **52**, 299.  
 Spencer, J. H., Johnston, K. J., Moran, J. M., Reid, M. J., and Walker, R. C. 1979, *Ap. J.*, **230**, 449.  
 Witzel, A., and Johnston, K. J. 1982, *Abh. Hamburger Sternw.*, **3**, 151.  
 Wolff, R. S., and Carlson, E. F. 1982, *Ap. J.*, **257**, 161.

P. F. BOWERS, K. J. JOHNSTON, and J. H. SPENCER: Code 4130, Naval Research Laboratory, Washington, DC 20375-5000